LANGMUIR

pubs.acs.org/Langmuir Article

Understanding the Retention of Vaping Additives in the Lungs: Model Lung Surfactant Membrane Perturbation by Vitamin E and Vitamin E Acetate

Published as part of Langmuir virtual special issue "Highlighting Contributions from our Editorial Board Members in 2023".

Panagiota Taktikakis, Mathieu Côté, Nivetha Subramaniam, Kailen Kroeger, Hala Youssef, Antonella Badia, and Christine DeWolf*

Cite This: *Langmuir* 2024, 40, 5651–5662 Read Online

ACCESS | Metrics & More | Article Recommendations | Supporting Information

ABSTRACT: Deviations from the normal physicochemical and functional properties of pulmonary surfactants are associated with the incidence of lung injury and other respiratory disorders. This study aims to evaluate the alteration of the 2D molecular organization and morphology of pulmonary surfactant model membranes by the electronic cigarette additives α-tocopherol (vitamin E) and α-tocopherol acetate (vitamin E acetate), which have been associated with lung injury, termed e-cigarette or vaping-use-associated lung injury (EVALI). The model membranes used contained a 7:3 molar ratio of DPPC (1,2-dipalmitoyl-*sn*-glycero-3-phosphocholine) and POPG (1-palmitoyl-2-oleoyl-*sn*-glycero-3-phosphoglycerol) to which α-tocopherol and α-tocopherol acetate were added to form mixtures of up to 20 mol % additive. The properties of the neat tocopherol additives and DPPC/POPG (7:3) mixtures with increasing molar proportions of additive were evaluated by surface pressure−area isotherms, excess area calculations, Brewster angle microscopy, grazing incidence X-ray diffraction, X-ray reflectivity, and atomic force microscopy. The addition of either additive alters the essential phase balance of the model pulmonary surfactant membrane by generating a greater proportion of the fluid phase. Despite this net fluidization, both tocopherol additives have space-filling effects on the liquid-expanded and condensed phases, yielding negative excess areas in the liquid-expanded phase and reduced tilt angles in the condensed phase. Both tocopherol additives alter the stability of the fluid phase, pushing the eventual collapse of this phase to higher surface pressures than the model membrane in the absence of an additive.

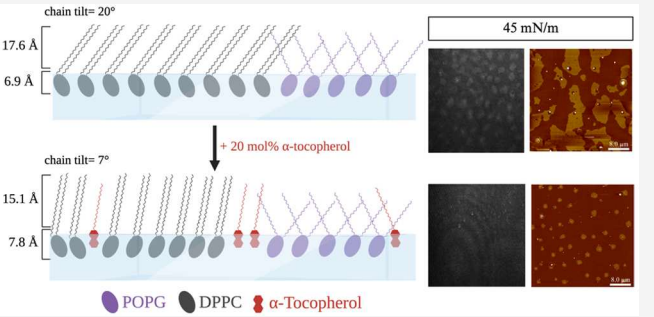

INTRODUCTION

The use of electronic cigarettes or "vaping" has grown significantly in popularity in recent years. At the start of 2019, a marked increase in the incidence of serious lung injuries associated with vaping in young adults with no pre-existing respiratory diseases challenged the common perception that vaping is a healthier alternative to smoking.[1] The medical condition of these young adults with lung injuries was labeled by the Centers for Disease Control and Prevention (CDC) as electronic cigarette or vaping product use-associated lung injury (EVALI). The CDC announced that this outbreak was strongly linked to the presence of α-tocopherol acetate (vitamin E acetate), a diluent in vaping solutions containing tetrahydrocannabinol. α-Tocopherol acetate was detected in bronchoalveolar lung lavage specimens from 94% of patients presenting with EVALI.[1,2] Current evidence is insufficient to rule out other contributing factors, but the molecular mechanism of lung injury from α-tocopherol (vitamin E) and its acetate form on the lungs requires further understanding.

Most of the literature on α-tocopherol−lipid interactions focuses on the miscibility of α-tocopherol in membrane bilayers to determine its preferential association with either saturated or unsaturated lipids to understand its biological importance as an antioxidant. DiPasquale et al. proposed that α-tocopherol more readily associates with disordered phospholipid environments, exhibiting a reduced partial molar volume in bilayers and favorable intermolecular interactions

Received: October 1, 2023
Revised: February 18, 2024
Accepted: February 19, 2024
Published: March 4, 2024

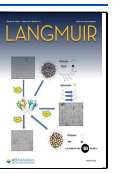

https://doi.org/10.1021/acs.langmuir.3c02952
Langmuir 2024, 40, 5651−5662

that correlate with the degree of chain unsaturation.[3] Jurak et al. studied monolayer models consisting of binary mixtures of α-tocopherol (20−75 mol %) and different phosphocholines, namely, dipalmitoylphosphatidylcholine (DPPC), palmitoyloleoylphosphatidylcholine (POPC), and dioleoylphosphatidylcholine (DOPC).[4] They also concluded that there is a correlation between the degree of unsaturation and the strength of the attractive interactions, with the diunsaturated DOPC exhibiting the strongest interactions, followed by the monounsaturated POPC, and then the saturated DPPC. However, despite these different interaction strengths, α-tocopherol showed a tendency to partially mix with all phosphocholines regardless of their unsaturation level.

In contrast to the experimental findings, molecular dynamics simulations by Leng et al. suggest that α-tocopherol preferentially associates with monounsaturated over polyunsaturated phospoholipids.[5] This preferential association with monounsaturated compared to polyunsaturated phospholipids is similar to the behavior of cholesterol, except that cholesterol shows an even greater affinity for saturated over monounsaturated phospholipids. Muddana et al. showed by computing the radial pair density of α-tocopherol in 1:1 mixtures of DPPC and diundecanoylphosphatidylcholine (DUPC) that α-tocopherol preferentially partitions to the phase boundary between the gel and fluid phases (under conditions of phase separation), thus acting as a lineactant.[6] They also noted that the previously reported preferential association of tocopherol with polyunsaturated fatty acid chains may not be generalizable and is also influenced by the positions of the units of unsaturation. Lineactants lead to a reduction of the line tension, favoring the formation of smaller domains. Experimental studies also suggest that α-tocopherol exhibits lineactant properties at added concentrations above 10 mol %.[3]

Pulmonary surfactant consists of 90% by weight of lipids, of which 70−80 mol % are saturated (with zwitterionic DPPC as the major component) and 30% are unsaturated with a high proportion of anionic phosphoglycerols such as palmitoyloleoylphosphatidylglycerol (POPG).[7] Binary mixtures of DPPC and POPG are commonly used as model membranes[8−11] because they mimic the saturated−unsaturated balance, the charged nature, the phase separation, and many of the functional properties of natural pulmonary surfactant extracts. Such simplified lipid-only models allow probing of the interaction of α-tocopherol, a lipid analogue, with various phospholipid phases formed in monolayer films. In this work, we have studied the impact of both α-tocopherol and its acetate form on the surface activity, morphology, compressibility, and structure of a model pulmonary surfactant membrane.

EXPERIMENTAL SECTION

Materials. 1,2-Dipalmitoyl-*sn*-glycero-3-phosphatidylcholine (DPPC, 99%) and 1-palmitoyl-2-oleoyl-phosphatidylglycerol (POPG, 99%) were purchased from Avanti Polar Lipids in a powder form. α-Tocopherol, α-tocopherol acetate (both 96%), tris-(hydroxymethyl)aminomethane (Tris, 99.8%), and NaCl (99%) were purchased from Sigma-Aldrich. ACS-grade chloroform (Fischer Scientific) was used to prepare the phospholipid and additive stock spreading solutions. All reagents were used without further purification. The molecular structures of the phospholipids and additives are shown in Figure 1.

Lipid Mixtures and Aqueous Subphases. Stock solutions of 1.0 mM DPPC and 1.0 mM POPG in chloroform were combined to prepare a solution containing a 7:3 molar ratio of DPPC and POPG.

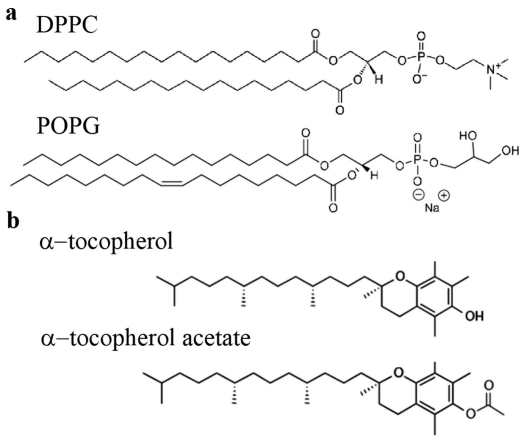

Figure 1. Molecular structures of the (a) phospholipids (DPPC and POPG) and (b) additives (α-tocopherol and α-tocopherol acetate, also known as vitamin E and vitamin E acetate) used in this work.

Stock solutions of α-tocopherol (1.0 mM) and α-tocopherol acetate (1.0 mM) in chloroform were combined with the DPPC:POPG (7:3) solution to prepare solutions containing 1, 5, 10, 15, and 20 mol % α-tocopherol or α-tocopherol acetate and 99, 95, 90, 85, and 80 mol % DPPC:POPG (7:3), respectively. Tris-buffered saline (TBS) comprising 50 mM Tris and 150 mM NaCl served as the aqueous subphase for all Langmuir monolayer experiments and was prepared with ultrapure water (resistivity of 18.2 MΩ cm) and pH adjusted to 7.4 using hydrochloric acid.

Surface Pressure−Molecular Area Isotherms. Surface pressure−molecular area isotherms were obtained using a Langmuir film balance (Model 516, Nima Technology) with a maximum trough surface area of 80 cm^2 and a filter paper Wilhelmy plate (Whatman No. 3001-604). Neat α-tocopherol, neat α-tocopherol acetate, DPPC:POPG (7:3), and their mixtures were spread on the TBS subphase, and the solvent was allowed to evaporate (10 min) prior to lateral symmetric compression of the film at the air−aqueous interface at a rate of 5 cm^2/min (equivalent to 6−7.5 $Å^2$/molecule/min, depending on the film). All experiments were conducted at room temperature (22.5 ± 0.5 °C), and at least three separate isotherms were obtained for each lipid composition to ensure reproducibility. Previous reports[12] have shown that the phase behavior of the model membranes at room temperature to be qualitatively similar to those at physiological temperatures, albeit with the phase transitions shifted to lower surface pressures.

The impact of the lipid composition on molecular mixing was assessed from changes to the average molecular area. The ideal mixing molecular area at a given pressure is calculated from the weighted average of the measured molecular areas of the DPPC:POPG (7:3) mixture and either neat α-tocopherol or α-tocopherol acetate. The excess molecular area (deviation from the ideal molecular area) can be calculated as follows:

$$A_{ideal} = (1 - \chi_{additive}) \times A_{DPPC:POPG(7:3)} + \chi_{additive} A_{additive} \quad (1)$$

$$A_{excess} = A_{measured} - A_{ideal} \quad (2)$$

where $\chi_{additive}$ is the mole fraction of additive in the mixture, $A_{DPPC:POPG(7:3)}$ is the molecular area of DPPC:POPG (7:3) at a given pressure, $A_{additive}$ is the molecular area of the neat additive monolayer at a given pressure, $A_{measured}$ is the experimental molecular area of DPPC:POPG (7:3) with additive, and A_{ideal} is the ideal mixing molecular area.

Brewster Angle Microscopy (BAM) Imaging. BAM imaging of monolayers at the air−aqueous interface during barrier compression was performed using an I-Elli2000 imaging ellipsometer (Nanofilm Technologies) coupled to a Langmuir film balance (Model 601BAM, Nima Technology) with a maximum trough area of 146 cm^2. The instrument is equipped with a 50 mW Nd:YAG laser (λ = 532 nm),

https://doi.org/10.1021/acs.langmuir.3c02952
Langmuir 2024, 40, 5651−5662

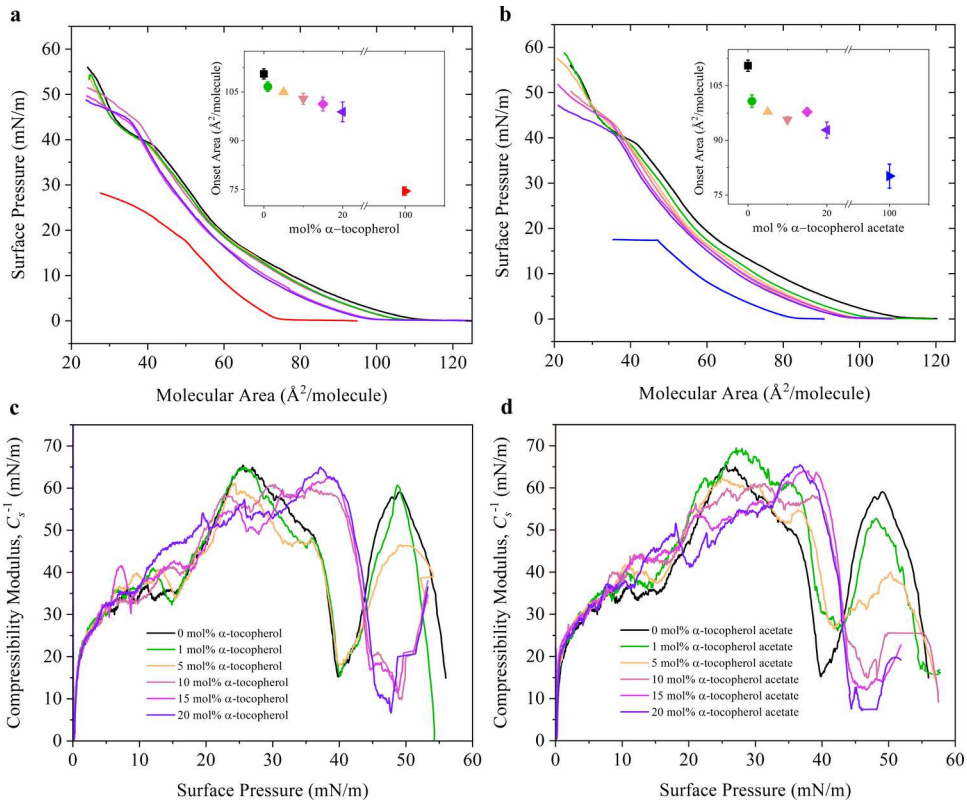

Figure 2. Upper panels: surface pressure–area isotherms for (a) neat α-tocopherol (red) and DPPC:POPG (7:3) mixtures with increasing molar concentrations of α-tocopherol (0, 1, 5, 10, 15, and 20 mol %, colors indicated in legend) and (b) neat α-tocopherol acetate (blue) and DPPC:POPG (7:3) mixtures with increasing molar concentrations of α-tocopherol acetate (0, 1, 5, 10, 15, and 20 mol %, colors indicated in legend). The insets show the variation in onset area as a function of the mole fraction of the additive. Lower panels: the compressibility moduli as a function of the surface pressure for DPPC:POPG (7:3) mixtures with (c) α-tocopherol and (d) α-tocopherol acetate.

and the images were captured using a 20× objective (with a field of view of 220 μm × 275 μm and a lateral resolution of approximately 1 μm) at the Brewster incident angle of 53.15°. Following a wait time of 10 min for solvent evaporation after spreading of the lipid solution, the monolayer was symmetrically compressed at a rate of 5 cm^2/min. All BAM images were obtained at 50% laser brightness intensity except for the images of the neat α-tocopherol, and α-tocopherol acetate monolayers that were obtained at 70% intensity.

Langmuir Monolayer Transfer onto the Mica Substrate. Monolayer films were vertically transferred on the upstroke from the air–aqueous interface onto freshly cleaved mica using the Langmuir–Blodgett technique. The monolayer was compressed and held for 5 min at the target pressure prior to transfer at a rate of 5 mm/min. The solid-supported films were allowed to dry under ambient conditions for 30 min and imaged by AFM within 24 h of their preparation.

Atomic Force Microscopy (AFM). A MultiMode 8HR scanning probe microscope (Bruker Nano, Santa Barbara, CA) was used to capture AFM images in Peak Force Tapping Mode in air with silicon tips mounted on nitride levers of a nominal spring constant of 0.4 N/m and a resonance frequency of 70 kHz (Model Scanasyst-Air, Bruker AFM Probes). Images were recorded at a scan rate of 0.759 Hz and 512 × 512-pixel resolution and processed with Nanoscope software, version 2.0. The condensed phase domains were identified by applying a height threshold and bearing analysis used to determine the percent area coverage of the condensed phase. Analyses were performed on at least three images randomly selected across multiple samples.

Grazing Incidence X-Ray Diffraction (GIXD). The GIXD experiments were performed at beamline 15-ID-C ChemMatCARS of the Advanced Photon Source (APS) at Argonne National Laboratory with the following parameters: an X-ray beam wavelength of 1.239 Å, an incidence angle of 0.0906°, a horizontal size of 20 μm, and a vertical size of 120 μm, leading to a beam footprint of 2 × 10^{-3} cm by 7.6 cm. The detector used was the 2D Swiss Light source PILATUS 100 K set to the single-photon counting mode. Two sets of slits, one placed in front of the detector to control the beam footprint and the other placed 280 mm from the sample, were used to minimize intense low-angle scattering. Experiments were performed at the air–aqueous interface of a 340 cm^2 Langmuir trough with a compression rate of 5 cm^2/min. The measured GIXD data are plotted as contour plots of the intensity as a function of both the horizontal (Q_{xy}) and the vertical (Q_z) scattering vector components. The lattice spacing d_{hk} was obtained from the in-plane diffraction data as $d_{hk} = 2\pi/Q^{hk}_{xy}$, where the Miller indices h and k were used to index the Bragg peaks needed to calculate the unit cell parameters for the in-plane lattice. The full width at half-maximum (fwhm) of the Bragg peaks after correction for the instrumental resolution (0.0084 Å^{-1}) was used to calculate the in-plane correlation length using the Scherrer formula as follows:

$$\xi_{xy} = 0.9 \times 2\pi \Big/ \mathrm{fwhm}_{\mathrm{intrinsic}}(Q_{xy}) \tag{3}$$

GIXD experiments were performed at lateral surface pressures of 10, 18, 35, and 45 mN/m and at a temperature of 22.0 ± 0.5 °C.

X-Ray Reflectivity (XR). XR is measured as a function of the vertical scattering vector component (Q_z). XR probes the electron density variation $\rho(z)$ of the vertical structure of the layers at the air–aqueous interface. The monolayer was modeled as a stack of slabs with each slab having a constant thickness and electron density. The electron density profile $\rho(z)$ was laterally averaged over both the ordered and disordered parts of the monolayer under the footprint of the X-ray beam.

The X-ray reflectivity data was analyzed using open-source (Python) software developed and provided by Wei Bu, beamline scientist at ChemMatCARS. The measured X-ray reflectivity $R(Q_z)$ is

https://doi.org/10.1021/acs.langmuir.3c02952
Langmuir 2024, 40, 5651–5662

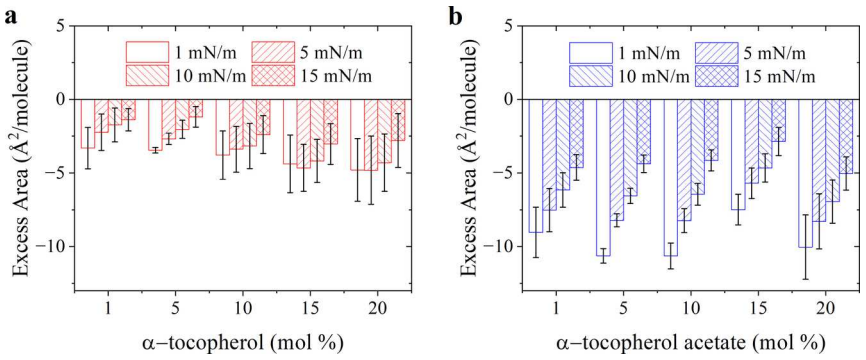

Figure 3. Molecular area deviations from the ideal mixing area (excess areas) for DPPC:POPG (7:3) mixtures containing (a) α-tocopherol and (b) α-tocopherol acetate at surface pressures of 1, 5, 10, and 15 mN/m. The standard deviations were calculated from triplicate measurements of the surface pressure−molecular area isotherms.

normalized by the Fresnel reflectivity $R_F(Q_z)$, which is calculated for a sharp air−aqueous interface. The X-ray reflectivity was calculated using the Parratt method. Nonlinear least-squares fitting was used to determine the minimum number (N^{-1}) of internal slabs to best fit the X-ray reflectivity data. In our XR data analysis, all systems were treated as a homogeneous monolayer film, although lateral phase separation occurs under the experimental conditions. This assumption was made based on the sizes of the condensed and liquid-expanded phases, which are less than the footprint of the X-ray beam in all our systems. This assumption has been previously used in the literature, where the domain sizes of the phase-separated patches are smaller than the X-ray beam footprint.[13] All XR experiments were performed at a lateral surface pressure of 35 mN/m and at a temperature of 22.0 ± 0.5 °C.

RESULTS AND DISCUSSION

Surface Pressure−Molecular Area Isotherms. The compression isotherms of the model lung surfactant mixture DPPC:POPG (7:3), α-tocopherol, α-tocopherol acetate, and mixtures of DPPC:POPG (7:3) and either α-tocopherol or α-tocopherol acetate are shown in Figure 2a,b. For DPPC:POPG (7:3), the onset area is 108 Å^2/molecule, while those of α-tocopherol and α-tocopherol acetate are much smaller, 74 and 80 Å^2/molecule, respectively. The onset areas of DPPC:POPG (7:3) mixtures containing varying molar concentrations of α-tocopherol or α-tocopherol acetate decreased with increasing concentration of additive, with a more pronounced effect observed with α-tocopherol acetate (Figure 2a,b insets). In particular, a shift of the DPPC:POPG isotherm to lower molecular areas is observed in the presence of both additives at concentrations ≥10 mol %.

DPPC:POPG mixtures are known to phase separate into a DPPC-rich condensed phase and POPG-rich liquid-expanded phase.[14,15] This phase transition can be difficult to discern from the isotherm, but its onset is associated with a minimum in the compressibility modulus versus surface pressure plots (Figure 2c,d) observed at around 13 mN/m. Beyond this pressure, the film remains phase separated until the collapse of the POPG-rich fluid phase, evident as a plateau in the isotherm at 42−45 mN/m, after which the surface pressure increases more steeply until the eventual film collapse at 55−60 mN/m (Figure 2a,b). By contrast, both α-tocopherol and α-tocopherol acetate films collapse at lower pressures, namely, below 20 mN/m. An elevated collapse pressure for mixtures of phospholipids and additives compared to the pure additives suggests an interaction between components.[3] The pressure for the collapse of the POPG-rich fluid phase is shifted to higher values in the presence of 10 mol % or more of the additive, indicative of stabilizing interactions between the tocopherol or tocopherol acetate and POPG. α-Tocopherol was shown to have a stabilizing effect on disordered bilayers wherein it suppressed the bilayer thermal expansivity.[16]

A direct comparison of the isotherms for a given concentration of additive is provided in Figure S1 of the Supporting Information. The isotherms of monolayers containing 0, 1, and 5 mol % additive are qualitatively similar in shape. At or above 10 mol % additive, there is a distinct change in the plateau pressure, which is shifted to higher values. As the proportion of additive increases, the slope change associated with the formation of a DPPC-rich condensed phase, which typically occurs around 13 mN/m in DPPC:POPG (7:3), becomes less pronounced in both the isotherm and compressibility plots, suggesting that α-tocopherol and α-tocopherol acetate are fluidizing the condensed DPPC-rich phase, as was observed with monolayers of DPPC and α-tocopherol, wherein the addition of 25−75 mol % α-tocopherol results in the disappearance of the liquid-expanded-to-condensed phase transition.[4]

Compressibility moduli (C_s^{-1}) for the neat α-tocopherol and α-tocopherol acetate films are presented in Figure S2, and the maximum C_s^{-1} are 55 and 47 mN/m, respectively. As a consequence of the methyl branching, the tocopherol phytyl side chains have an inherently larger cross-sectional area than an unbranched chain. Yasmann and Sukharev demonstrated that branched alkyl chains, such as DPhPC (diphytanoylphosphatidylcholine) (the branched lipid equivalent of DPPC), exhibited a lower film compressibility modulus of 115 mN/m[17] than DPPC for which the film compressibility modulus can reach values of up to 250 mN/m.[18] Additionally, the shorter chain length of the tocopherols may also contribute to the low compressibility, for example, the 14-carbon saturated DMPC (1,2-dimyristoyl-*sn*-glycero-3-phosphocholine) exhibits a maximum film compressibility modulus value of 100 mN/m,[19] which is lower than that of the 16-carbon DPPC film. At all surface pressures up to collapse, the α-tocopherol film compressibility modulus is distinctly higher than that of the α-tocopherol acetate film, despite the similarity of the isotherm shapes. This is attributed to the acetate (as opposed to hydroxyl) in the headgroup altering the molecular orientation of the α-tocopherol acetate at the interface. The C═O portion of the ester functional groups present on the headgroups of surface-active molecules has been reported to be mainly oriented parallel to the aqueous surface or subphase.[20] An altered molecular orientation can affect not only the neat film

https://doi.org/10.1021/acs.langmuir.3c02952
Langmuir 2024, 40, 5651−5662

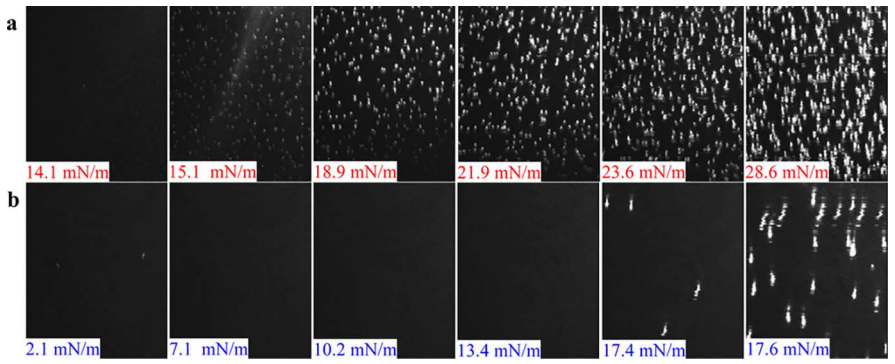

Figure 4. BAM images (220 μm × 275 μm) of monolayers at the air−aqueous interface of (a) α-tocopherol and (b) α-tocopherol acetate as a function of the surface pressure.

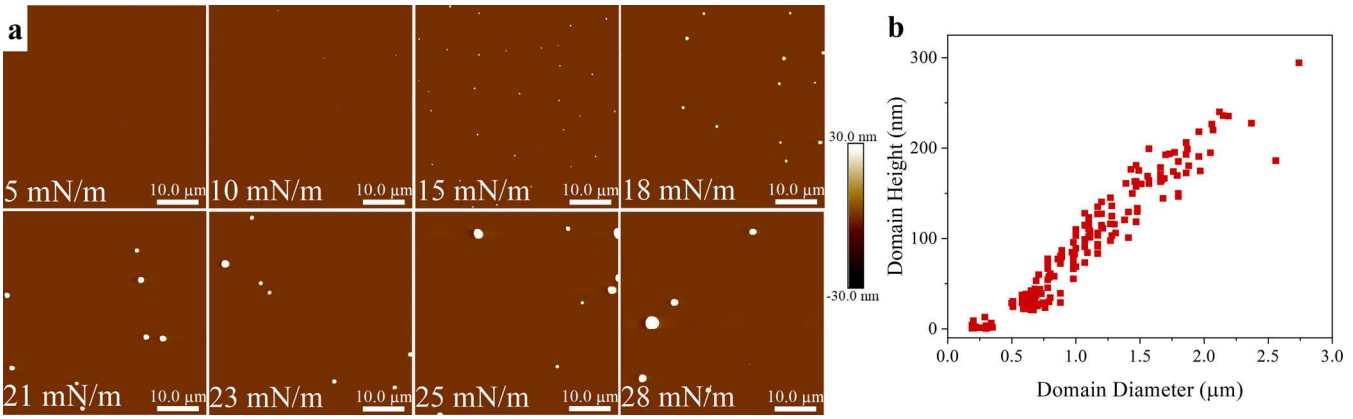

Figure 5. (a) AFM images of α-tocopherol at surface pressures of 5, 10, 15, and 18 mN/m (top row) and 21, 23, 25, and 28 mN/m (bottom row). (b) Corresponding domain diameter and height showing the growth of the domains both in width and height as the surface pressure increases.

compressibility but also its miscibility with different lipids and monolayer phases.

Deviations from Ideal Mixing. To assess the phospholipid−tocopherol additive interactions in the mixed monolayers, excess molecular areas were calculated for varying molar concentrations of α-tocopherol (Figure 3a) and α-tocopherol acetate (Figure 3b). Positive deviations suggest repulsive interactions and film expansion, while negative deviations indicate attractive interactions and/or condensation.[21] Excess areas were calculated at surface pressures of 1−15 mN/m since monolayers of α-tocopherol and α-tocopherol acetate collapse by 18 mN/m. For the α-tocopherol mixtures, small negative deviations less than 5 Å^2/molecule are observed, which decrease as the film is compressed, indicating the presence of attractive interactions between the model membrane and α-tocopherol. In general, it appears that the deviations are more pronounced as the proportion of α-tocopherol increases; however, these increases may not be statistically significant, given the reported errors. We speculate that the additive has a greater space-filling impact on the chains when the molecular spacing is higher. As the film is compressed, the chains naturally extend more, and there is less opportunity for the α-tocopherol to space-fill.

In contrast to α-tocopherol, the addition of just 1 mol % α-tocopherol acetate results in a significant condensing effect with negative excess areas of −9 ± 2 Å^2/molecule, for which the decrease in excess area as the film is compressed is also more pronounced. In summary, increasing the molar concentration of either additive leads to a negative deviation from the ideal mixing molecular areas, with the deviation being more pronounced at lower pressures, i.e., when all components are in the liquid-expanded phase and for mixtures containing α-tocopherol acetate. The substitution of the hydroxyl group with an acetate clearly had a significant impact.

A larger impact of α-tocopherol acetate on DPPC:POPG (4:1), compared to α-tocopherol, was also observed by van Bavel et al.[22] Their phospholipid-additive isotherms are, however, shifted to molecular areas greater than that of DPPC:POPG, despite smaller molecular areas for the single-chain α-tocopherol and α-tocopherol acetate. For comparison purposes, we estimate excess areas of +6 Å^2/molecule (5 mN/m), + 9 Å^2/molecule (10 mN/m), and +10 Å^2/molecule (20 mN/m) with just 5 mol % additive using our tocopherol additive isotherms (since neat α-tocopherol and α-tocopherol isotherms were not reported by the authors). The excess areas will be addressed further in the context of morphology in the next section.

Film Morphology. The morphologies of neat α-tocopherol and α-tocopherol acetate films imaged by using BAM are illustrated in Figure 4. α-Tocopherol initially forms a homogeneous film at low pressure. At 14 mN/m, small, very low contrast domains begin to appear. As the film is further compressed, the α-tocopherol begins to collapse and three-dimensional aggregates (protrusions) form, evident as bright spots in the BAM images, in agreement with previous studies.[4,22] These protrusions increase in diameter and brightness with compression, a growth pattern that likely leads to broad collapse over a range of surface pressures

https://doi.org/10.1021/acs.langmuir.3c02952
Langmuir 2024, 40, 5651−5662

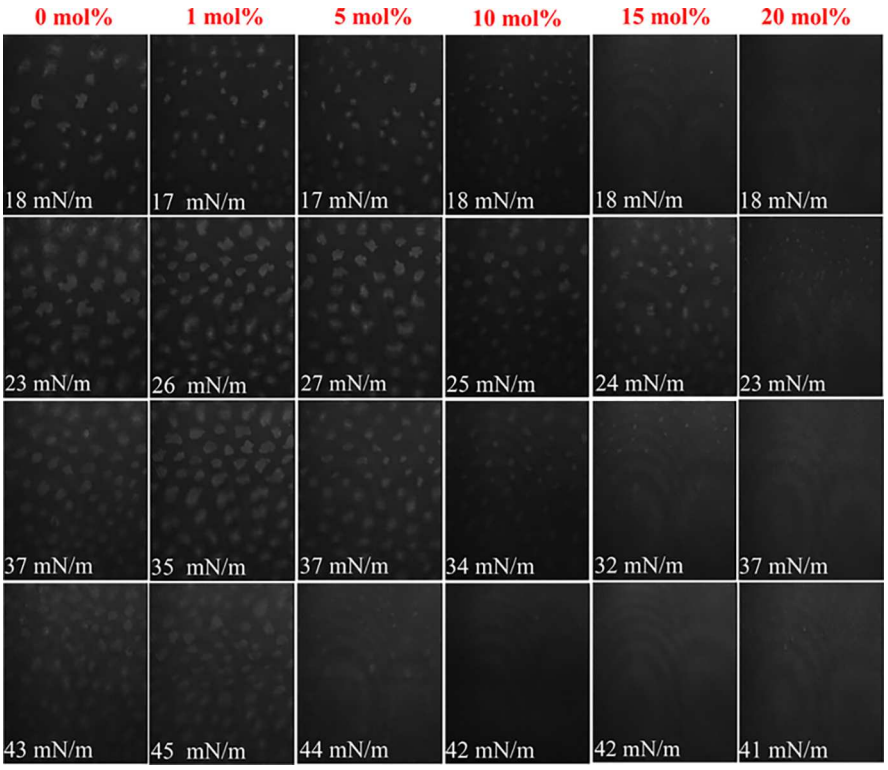

Figure 6. BAM images (220 μm × 275 μm) of DPPC:POPG (7:3) as a function of the surface pressure (from top to bottom): ∼18, ∼25, ∼35, and ∼45 mN/m, and with varying molar concentrations of added α-tocopherol added (from left to right): 0, 1, 5, 10, 15, and 20 mol %.

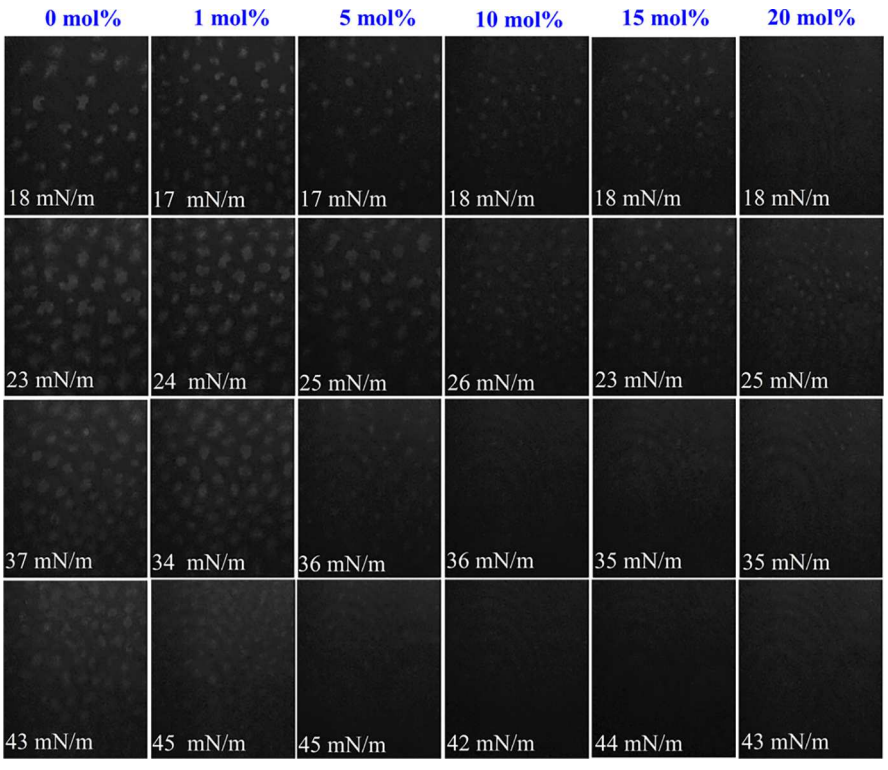

Figure 7. BAM images (220 μm × 275 μm) of DPPC:POPG (7:3) as a function of the surface pressure (from top to bottom): ∼18, ∼25, ∼35, and ∼45 mN/m, and with varying molar concentrations of added α-tocopherol acetate (from left to right): 0, 1, 5, 10, 15, and 20 mol %.

observed in the isotherm. AFM images confirm a homogeneous phase below 15 mN/m (Figure 5a). The diameter of the protrusions observed at pressures ≥15 mN/m directly correlates with the height (Figure 5b).

In contrast to α-tocopherol (Figure 2a), the isotherm α-tocopherol acetate shows a sharp collapse at 17.5 mN/m (Figure 2b), which correlates with the immediate formation of fewer but larger very bright protrusions from the monolayer

https://doi.org/10.1021/acs.langmuir.3c02952
Langmuir 2024, 40, 5651−5662

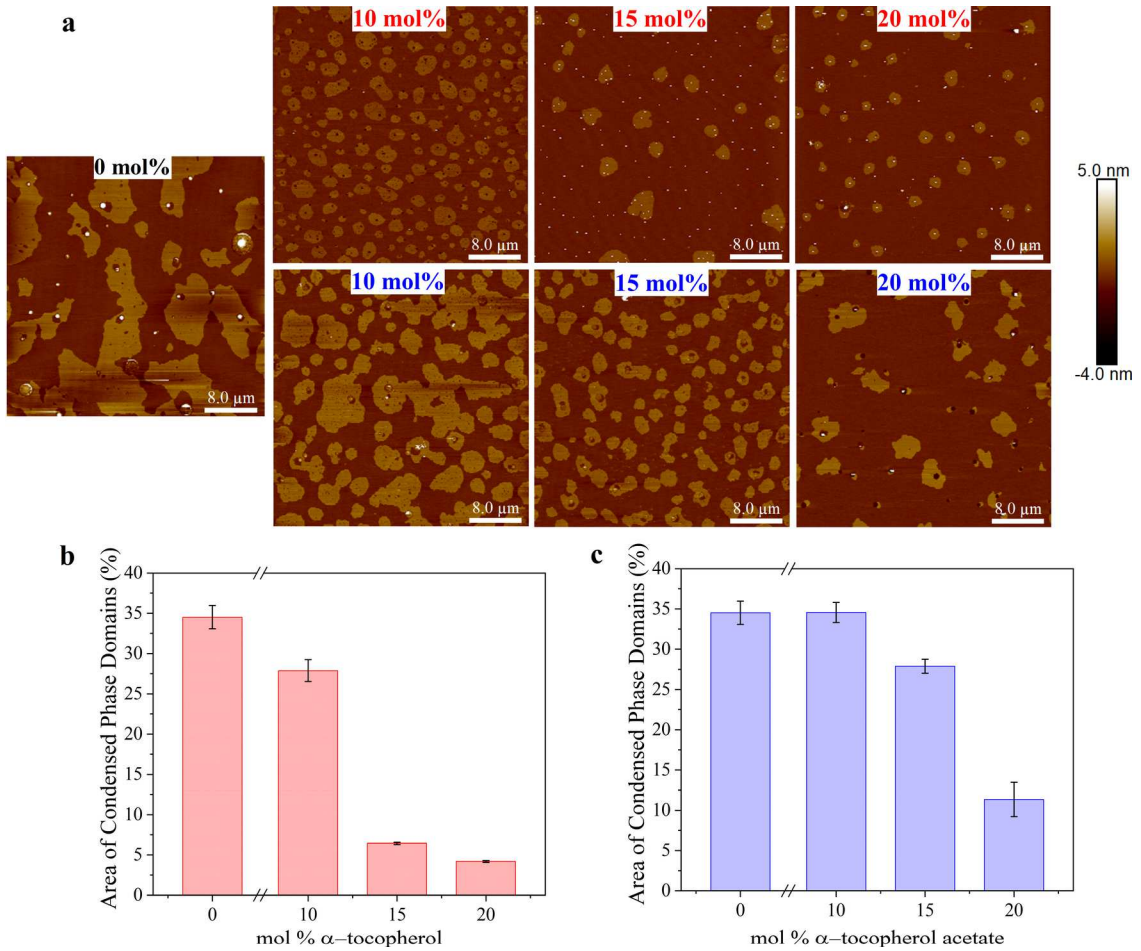

Figure 8. (a) AFM images of monolayer films transferred onto mica at 45 mN/m for DPPC:POPG (7:3) (black, 0 mol %) and varying molar concentrations (10, 15, and 20 mol %) of added α-tocopherol (red, top) and α-tocopherol acetate (blue, bottom). Corresponding % area coverage of condensed phase domains for DPPC:POPG (7:3) monolayer films with different molar concentrations of added (b) α-tocopherol or (c) α-tocopherol acetate.

film (Figure 4b). The sharp collapse makes Langmuir−Blodget transfer at constant pressure difficult, and AFM images of such films transferred at both 10 and 17.5 mN/m exhibit a flat, uniform, and featureless surface with no visible protrusions (data not shown). The difference in collapse is related to the kinetics of the growth of the protrusions, for which the altered molecular orientation (due to the replacement of a hydroxyl by an acetate) and consequent film compressibility modulus (as discussed earlier) play a determining role.

The BAM images of the DPPC:POPG (7:3) monolayer show the appearance of classical condensed phase domains at around 18 mN/m that persist at high pressures (Figures 6 and 7). These domains are attributed to a DPPC-rich condensed phase surrounded by a POPG-rich fluid phase. At higher pressures, there is a loss in optical contrast, which will be discussed later. A little change in the film morphology is observed with the addition of 1 and 5 mol % α-tocopherol or α-tocopherol acetate to the DPPC:POPG (7:3) mixture. At best, there is a minor variation in the domain sizes since some domains appear to be slightly larger at equivalent surface pressures. This may be explained by subtle changes in the line tension of the DPPC-rich condensed domains, where higher line tensions drive the formation of larger domains, and lower line tensions drive the formation of smaller domains.[23] Both a loss in optical (phase) contrast and the reduction of the total condensed phase areas occur at lower surface pressures with greater concentrations of the additives, specifically above 10 mol % for α-tocopherol and 5% mol for α-tocopherol acetate, suggesting a fluidization of the monolayer film. Additionally, the bright protrusions formed by the tocopherols are eliminated in the mixed films, in agreement with the isotherm that shows no indication of an independent collapse of the tocopherol phase.

The reduction in contrast observed at higher compression states has previously been attributed to either the collapse of the fluid phase[24] or to the formation of nanoscale domains below the optical resolution of BAM.[25] To determine if the loss of contrast can be attributed to fluidization or one of the aforementioned factors, DPPC:POPG:α-tocopherol films were transferred onto mica for AFM analysis (Figure 8). An analysis of the surface area occupied by the condensed phase domains reveals a 35% area coverage of the condensed phase in the absence of α-tocopherol that is reduced to 4% with 20 mol % α-tocopherol, indicative of fluidization. A distinct step change in the condensed phase coverage occurs for proportions of α-tocopherol greater than 10 mol %. Additionally, by 20 mol % α-tocopherol, most of the domain diameters are between 0.5 and 1.5 μm and, thus, below the lateral resolution of BAM, contributing to the loss of optical contrast. Muddana et al. showed that α-tocopherol exhibited lineactant properties such

https://doi.org/10.1021/acs.langmuir.3c02952
Langmuir 2024, 40, 5651−5662

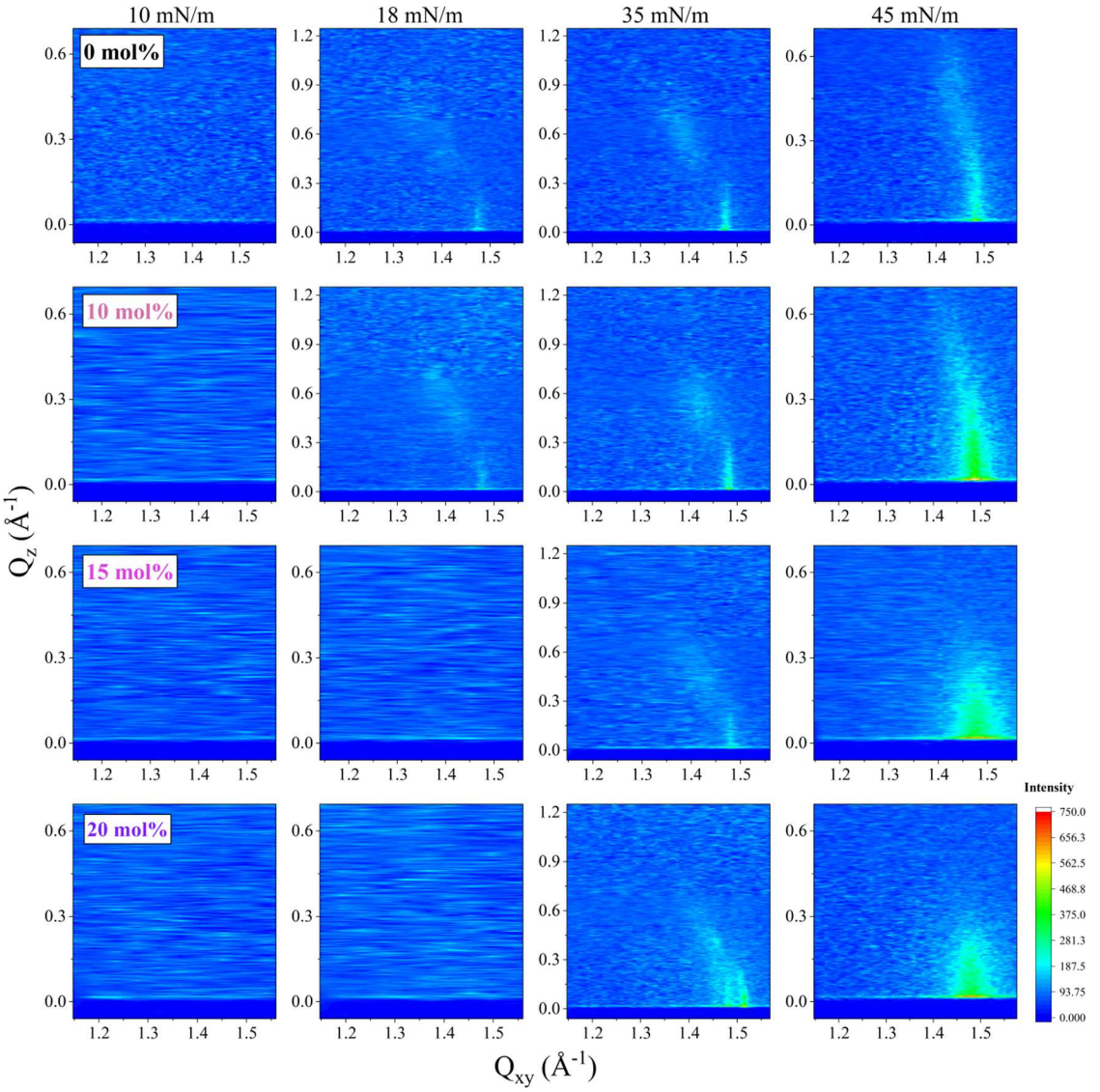

Figure 9. Contour plots of the X-ray intensities as a function of the in-plane (Q_{xy}) and out-of-plane (Q_z) scattering vector components for DPPC:POPG (7:3) with varying molar concentrations of α-tocopherol (top to bottom): 0, 10, 15, and 20 mol % at surface pressures (right to left) of 10, 18, 35, and 45 mN/m (note that not all Q_z scales are the same).

that it favored the phase boundaries in DPPC:DUPC (1:1) bilayers.[6] Lineactants reduce the line tension, lowering the energetic cost of forming phase boundaries and resulting in smaller domains.

With both phases present, the tocopherols likely partition between the two phases and generate competing effects in terms of the mean molecular area. The expansion observed by Van Bavel et al. may be related to the higher proportion (80%) DPPC in their model membrane.[22] The previously reported preferential partitioning of α-tocopherols into the fluid phase may drive the apparent fluidization. To understand the mixing effects on each of the individual phases, isotherms for 1:1 POPG:α-tocopherol (representing if all the tocopherol partitions to the fluid phase) and 3:1 DPPC:α-tocopherol (representing if all the tocopherol partitions to the condensed phase) were investigated (Figure S3) and the excess areas are tabulated in Table S1. POPG:α-tocopherol yields excess areas of -1 Å^2/molecule at 1 mN/m and -2 Å^2/molecule at 10 mN/m, while DPPC:α-tocopherol exhibits excess areas of -7 Å^2/molecule at 1 mN/m and +8 Å^2/molecule at 10 mN/m, respectively. This is in agreement with partial molar volume measurements that show a larger tocopherol partial molar volume in a DPPC fluid phase (above its T_m) than in a POPC fluid phase at the same temperature.[16] Notably, where each lipid forms a liquid-expanded phase, we have contraction of the film (all pressures for POPG, low pressures for DPPC). This contraction is significantly greater for saturated and zwitterionic DPPC lipids. Once the lipid film adopts a condensed phase (the plateau for DPPC is between 6 and 10 mN/m), there is a shift to film expansion. This can be due to either an expansion of the condensed phase or the prevention of this condensed phase from forming, wherein the DPPC molecules remain in a liquid-expanded phase to higher surface pressures. Although the values obtained would suggest that the tocopherols predominantly associate with the fluid phase, GIXD and XR were used to determine whether the tocopherols are miscible to any extent with the DPPC condensed phase (see below).

With increasing proportions of both additives, a fluidization of the condensed phase is observed at surface pressures above

https://doi.org/10.1021/acs.langmuir.3c02952
Langmuir 2024, 40, 5651−5662

18 mN/m. It is important to emphasize that the excess area calculations were restricted to surface pressures of up to 15 mN/m due to the low collapse pressures of α-tocopherol and α-tocopherol acetate. The BAM measurements were taken at surface pressures higher than 15 mN/m, rendering it impossible to accurately determine the precise impacts at these higher surface pressures. However, analogous to cholesterol, α-tocopherol contains major structural components, such as a rigid ring structure with a polar hydroxyl group at one end and a hydrophobic chain at the other end. The difference is that the chromanol group on α-tocopherol is smaller than the steroid moiety on cholesterol, and the phytyl side chain (13 carbons) on α-tocopherol is longer than the branched chain (5 carbons) on the sterol.[5] The addition of 1−30 mol % cholesterol to model surfactant monolayers comprising 8:2 DPPC:DPPG (1,2-dipalmitoyl-*sn*-glycero-3-phosphoglycerol) leads to the formation of smaller circular domains and decreased condensed phase area coverages.[26] Cholesterol induces a contraction in molecular area when mixed with saturated lipids like DPPC and a slight expansion when mixed with more unsaturated lipids like DOPC and POPC.[3] By analogy, α-tocopherol, like cholesterol, may have a larger impact on the condensed phase than on the fluid phase.

Film Structure. The GIXD contour plots obtained for DPPC:POPG (7:3) and their mixtures with α-tocopherol (molar concentrations of 10, 15, and 20 mol %) are shown in Figure 9. GIXD was performed at surface pressures of 10 mN/m (where DPPC:POPG (7:3) is in a liquid-expanded phase), 18 mN/m (where DPPC-rich condensed phase domains are first evident in BAM), and 35 and 45 mN/m (just below and above, respectively, the collapse/expulsion of the POPG-rich phase). At all pressures between 18 and 45 mN/m, the diffraction patterns of DPPC:POPG (7:3) show three low-order reflections (10, 01, $1\bar{1}$) with Bragg rod maxima above the horizon (Q_z) that correspond to an oblique lattice with tilted chains.[14] Note that GIXD peaks represent only the structure of the condensed phase domains since fluid- or liquid-expanded phases yield no diffraction. The condensed phase is attributed to a DPPC-rich phase given its similarity to the diffraction pattern of DPPC itself,[27] and the fact that POPG forms a liquid-expanded phase under these conditions. The peak positions and unit cell parameters calculated from fits of the three Bragg peaks and Bragg rods are listed in Tables S2 and S3. The DPPC-rich phase in the absence of α-tocopherol yields tilt angles of 31°, 28°, and 20° for pressures of 18, 35, and 45 mN/m, respectively. The large chain tilt angle of the DPPC-rich phase is comparable to the values reported in the literature[27] at similar surface pressures and is attributed to the area mismatch of the large DPPC headgroup and two alkyl chains.[28] By tilting the chains, a balance between the projected area of the chains and that of the phosphatidylcholine headgroup is achieved.[28]

The diffraction peaks for the mixtures containing 10, 15, and 20 mol % α-tocopherol at 35 mN/m confirm the presence of DPPC-rich condensed phase domains within a fluid POPG phase. The lack of diffraction peaks at 18 mN/m for 15 and 20 mol % indicates that the α-tocopherol hinders the formation of the condensed phase, pushing its formation to higher surface pressures. With increasing molar concentrations of α-tocopherol, the out-of-plane peaks move to lower Q_z and higher Q_{xy} values (Table S2), indicative of a tilt angle decrease from 28° (with no α-tocopherol) to 19° at 35 mN/m (with 20 mol % added α-tocopherol) (Table S3), evidence that α-tocopherol intercalates in the DPPC chain region and mimics the behavior of low amounts of cholesterol in PC membranes.[29] By 45 mN/m, the diffraction peaks for systems with α-tocopherol shift to much lower Q_z values, corresponding to very low tilt angles. Like cholesterol, we suggest that α-tocopherol alleviates the area mismatch of the large DPPC headgroups by incorporating itself between the DPPC chains.[28,29] Thus, we propose that some of the α-tocopherol intercalate within the condensed DPPC phase, leading to a notable reduction in the tilt angle.

For DPPC:POPG (7:3) with 20 mol % α-tocopherol at 35 mN/m, additional peaks are observed at higher Q_z (Figure 9). Repetition of the measurement yielded diffraction peaks associated with the same DPPC-rich phase peaks but not the additional peaks at higher (>1.5 $Å^{-1}$) Q_{xy} (Figure S4). We attribute these high Q_{xy} peaks to a kinetic effect, wherein, as the POPG begins to collapse, the α-tocopherol redistributes between the phases (the partitioning of α-tocopherol between the remaining LE and condensed phase changes). Depending on the extent of loss of POPG and the kinetics of the molecular redistribution, an intermediate phase can form. By 45 mN/m, the film has had more time to equilibrate, and these higher Q_{xy} peaks are less distinct. A future study will investigate the partitioning of the α-tocopherol between these phases in more depth.

GIXD measurements on the DPPC:POPG:α-tocopherol acetate mixture were performed for only 20 mol % additive at surface pressures of 20, 35, and 45 mN/m and are shown in Figure S5. The fits and unit cell parameters are listed in Tables S2 and S3, respectively. Unlike the 20 mol % tocopherol system, by 20 mN/m, diffraction peaks from the emerging DPPC-rich condensed phase are observed. At 35 and 45 mN/m, the diffraction patterns from the DPPC-rich phase are weaker and with lower signal-to-noise, which may indicate that the acetate analogue of α-tocopherol induces a greater degree of fluidization (i.e., less condensed phase in the beam footprint). At 35 mN/m, the chain tilt angle for the 20 mol % α-tocopherol acetate mixture is approximately 12° (Table S3), considerably lower than that of DPPC:POPG (7:3) without any additives (28°) and considerably lower than that of the film analogue with 20 mol % α-tocopherol (19°). The addition of a simple acetate group to the α-tocopherol headgroup does not hinder its incorporation into the DPPC lattice and yields a significantly reduced alkyl chain tilt angle.

X-Ray reflectivity data were fit with the top slab representing the alkyl chains (tail) and a lower slab representing the headgroups to generate a vertical electron density profile (Figure 10). Fitting outputs are summarized in Table S4.

The presence of 15 or 20 mol % α-tocopherol in the DPPC:POPG (7:3) monolayer yields a smaller average alkyl chain thickness (15.1 Å) compared to that of DPPC:POPG (7:3) (17.6 Å). The film thickness represents the weighted average of both the liquid-expanded and condensed phases. The decrease in the alkyl chain thickness is most likely due to the increased proportion of the thinner liquid-expanded phase. The XR fits also indicate a larger average headgroup thickness with added α-tocopherol (7.8 Å) compared to that of DPPC:POPG (7:3) with no α-tocopherol (6.9 Å). Figure 11 depicts the aromatic moiety of α-tocopherol anchored to the subphase. The remainder of the chromanol ring is positioned above the phosphocholine headgroup of DPPC, which may explain the increase in headgroup thickness. This arrangement was previously observed by resonance energy transfer studies,

https://doi.org/10.1021/acs.langmuir.3c02952
Langmuir 2024, 40, 5651−5662

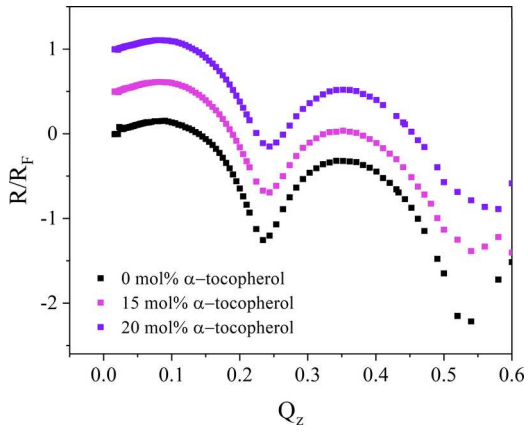

Figure 10. Normalized X-ray reflectivity versus the vertical scattering vector component Q_z of DPPC:POPG (7:3) in the absence and presence of 15 mol % α-tocopherol and 20 mol % α-tocopherol at a surface pressure of 35 mN/m.

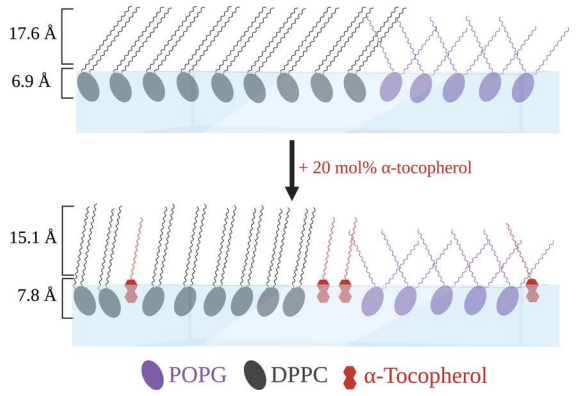

Figure 11. Schematic representation of α-tocopherol partitioning between the liquid-expanded and condensed phases.

with bilayers composed of 20 mol % α-tocopherol and DPPC.[30] Furthermore, the addition of 20 mol % α-tocopherol in DPPC:POPG (7:3) leads to an increase in electron density at the tail region while causing a reduction in electron density at the headgroup region. The α-tocopherol molecules within the DPPC-rich condensed phase contribute to an expansion of the intermolecular space between the DPPC headgroups, decreasing the overall headgroup electron density. The electron enrichment at the tail region can be the result of the incorporation of the branched phytyl chain of α-tocopherol within the alkyl chain region.

Implications of the Findings for EVALI. α-Tocopherol acetate has been found in significant proportions in the bronchoalveolar lavage (BAL) samples from EVALI patients.[2] The persistence of α-tocopherol acetate in BAL fluids indicates its retention in the alveoli. Given the lipophilic structure of α-tocopherol acetate, as well as its physical and chemical similarity to phospholipids, it is highly likely to embed in the pulmonary surfactant coating of the alveoli, the first line of defense to inhaled species. Our findings using model membranes, which show that α-tocopherol and α-tocopherol acetate are present in both the fluid and condensed phases of the pulmonary surfactant, are consistent with this retention in the alveoli and BAL fluids. EVALI patients presented clinical pathologies including ground-glass opacities[31,32] and foamy microphages,[33] as observed with exogenous lipid pneumonia. Thus, it has been suggested that EVALI represents a form of airway-centered chemical pneumonitis.[1,33] The increase in foamy macrophages is associated with impaired recycling of the pulmonary surfactant.[34] The pulmonary surfactant membrane composition is tightly regulated. Changes in its composition, in this case through the deposition of fatty materials (α-tocopherol and α-tocopherol acetate) and resulting impaired pulmonary surfactant recycling, are expected to cause difficulty in gas-exchange and breathing (due to changes in surface tension and the work of breathing).[35] The latter can contribute to a shortness of breath and the former to reduced oxygen levels, both commonly reported symptoms for EVALI.[31]

CONCLUSIONS

Herein, we have compared the phase behavior and interactions of α-tocopherol and α-tocopherol acetate with the different phases of lung surfactant model membranes. While qualitatively similar surface pressure−area isotherms and film morphologies are obtained, there are notable differences produced by replacing the hydroxyl in the headgroup with acetate. α-Tocopherol exhibits a higher compressibility than α-tocopherol acetate and an altered kinetics of the film collapse, with α-tocopherol exhibiting a broader collapse over a range of surface pressures that correlates with the slow growth (laterally and vertically) of protrusions comprising the expelled lipid material. By contrast, the collapse from the liquid-expanded phase of α-tocopherol acetate is very sharp and yields fewer but larger lipid protrusions.

The interaction of either α-tocopherol or α-tocopherol acetate with the model membrane lipids induces the tocopherols to stay in the plane of the membrane to much higher surface pressures, inhibiting the formation of the tocopherol-rich protrusions. Both tocopherols partition between the DPPC-rich condensed and POPG-rich LE phases. α-Tocopherol appears to take up some of the excess space within a liquid-expanded phase (negative excess areas for POPG at all pressures and DPPC at 1 and 5 mN/m) without inducing a condensed phase. The positive excess areas for DPPC:α-tocopherol mixtures at 10 and 15 mN/m combined with changes in the GIXD peak positions for the DPPC:POPG mixtures with either additive confirm that some α-tocopherol and α-tocopherol acetate clearly partition into the DPPC-rich condensed phase. The reduction in the alkyl chain tilt angle of the condensed phase indicates that the film expansion is not due to expansion of the condensed phase. Notably, higher concentrations of α-tocopherol acetate, compared with α-tocopherol, are required to see extensive fluidization of the film. This may be because the altered molecular orientation of α-tocopherol acetate enables better incorporation into the DPPC-rich phase, evidenced by the reduced fluidization and significantly lower tilt angles.

The biophysical properties and functionality of the pulmonary surfactant membrane are finely tuned to its composition and phase structure.[12] Both α-tocopherol and α-tocopherol acetate lead to a net fluidization of the model membranes by inhibiting the formation of the condensed phase, thus increasing the proportion of the liquid-expanded phase, despite having a contracting effect on each individual phase. This fluidization greatly diminishes the proportion of the condensed phase, whose role is to ensure the film stability at ultralow surface tension and high compression states (i.e., upon exhalation). This fluidization, along with the altered

https://doi.org/10.1021/acs.langmuir.3c02952
Langmuir 2024, 40, 5651−5662

collapse pressure, becomes most evident at α-tocopherol proportions greater than 10 mol % and α-tocopherol acetate proportions greater than 15 mol %. Dosimetry analysis has predicted that 42% of α-tocopherol acetate inhaled from e-liquids can deposit in the pulmonary rather than the tracheal region.[36] The residence time and accumulation of tocopherols as a function of vaping frequency in the pulmonary surfactant are not known, although tocopherol acetate was sufficiently present to be detectable in BAL fluids from patients with EVALI. Although studied herein in terms of their impact on model lung surfactant membranes, given α-tocopherol is a naturally occurring, membrane-soluble antioxidant, and α-tocopherol acetate is used not only as a vaping solution diluent but also as a prodrug precursor, the fluidizing effects of these compounds have broader implications.

■ ASSOCIATED CONTENT

Supporting Information

The Supporting Information is available free of charge at https://pubs.acs.org/doi/10.1021/acs.langmuir.3c02952.

Surface pressure area isotherms for additives/mixtures with POPG, DPPC, and DPPC:POPG; compressibility moduli for α-tocopherol and α-tocopherol acetate films; tabulated excess areas for additive mixtures with POPG and DPPC; additional GIXD data; tabulated GIXD (peak positions and unit cell parameters); and fitted parameters for X-ray reflectivity data (thicknesses and electron densities) (PDF)

■ AUTHOR INFORMATION

Corresponding Author

Christine DeWolf − *Department of Chemistry and Biochemistry and Centre for NanoScience Research, Concordia University, Montréal, Quebec H4B 1R6, Canada; FRQNT Quebec Centre for Advanced Materials, Montréal, Quebec H2X 2J6, Canada;* orcid.org/0000-0002-5185-7237; Email: christine.dewolf@concordia.ca

Authors

Panagiota Taktikakis − *Department of Chemistry and Biochemistry and Centre for NanoScience Research, Concordia University, Montréal, Quebec H4B 1R6, Canada; FRQNT Quebec Centre for Advanced Materials, Montréal, Quebec H2X 2J6, Canada*

Mathieu Côté − *Department of Chemistry and Biochemistry and Centre for NanoScience Research, Concordia University, Montréal, Quebec H4B 1R6, Canada; FRQNT Quebec Centre for Advanced Materials, Montréal, Quebec H2X 2J6, Canada*

Nivetha Subramaniam − *Department of Chemistry and Biochemistry and Centre for NanoScience Research, Concordia University, Montréal, Quebec H4B 1R6, Canada; FRQNT Quebec Centre for Advanced Materials, Montréal, Quebec H2X 2J6, Canada*

Kailen Kroeger − *Department of Chemistry and Biochemistry and Centre for NanoScience Research, Concordia University, Montréal, Quebec H4B 1R6, Canada; FRQNT Quebec Centre for Advanced Materials, Montréal, Quebec H2X 2J6, Canada*

Hala Youssef − *Department of Chemistry and Biochemistry and Centre for NanoScience Research, Concordia University, Montréal, Quebec H4B 1R6, Canada; FRQNT Quebec Centre for Advanced Materials, Montréal, Quebec H2X 2J6, Canada*

Antonella Badia − *Département de chimie and Institut Courtois, Université de Montréal, Montréal, Quebec H3C 3J7, Canada; FRQNT Quebec Centre for Advanced Materials, Montréal, Quebec H2X 2J6, Canada;* orcid.org/0000-0002-1026-4136

Complete contact information is available at: https://pubs.acs.org/10.1021/acs.langmuir.3c02952

Author Contributions

The manuscript was written through contributions of all authors. All authors have given approval to the final version of the manuscript.

Notes

The authors declare no competing financial interest.

■ ACKNOWLEDGMENTS

This research was supported by the Natural Sciences and Engineering Research Council of Canada (NSERC) through Grant Number RGPIN-2019-07043 (CD). P.T. is grateful for the support from the Chemistry and Biochemistry Department at Concordia University (Faculty of Arts and Science Graduate Fellowship—MSc program) and NSERC (Canada Graduate Scholarship—Master's—CGS-M). P.T., M.C., and K.K. acknowledge the support of NSERC via the Undergraduate Summer Research Awards (USRA) program. NSF's ChemMatCARS, Sector 15 at the Advanced Photon Source (APS), Argonne National Laboratory (ANL) is supported by the National Science Foundation under grant number NSF/CHE-1834750. This research used resources of the Advanced Photon Source, a U.S. Department of Energy (DOE) Office of Science User Facility operated for the DOE Office of Science by Argonne National Laboratory under Contract No. DE-AC02-06CH11357.

■ REFERENCES

(1) Duffy, B.; Li, L.; Lu, S.; Durocher, L.; Dittmar, M.; Delaney-Baldwin, E.; Panawennage, D.; LeMaster, D.; Navarette, K.; Spink, D. Analysis of Cannabinoid-Containing Fluids in Illicit Vaping Cartridges Recovered from Pulmonary Injury Patients: Identification of Vitamin E Acetate as a Major Diluent. *Toxics* **2020**, *8* (1), 8.

(2) Blount, B. C.; Karwowski, M. P.; Shields, P. G.; Morel-Espinosa, M.; Valentin-Blasini, L.; Gardner, M.; Braselton, M.; Brosius, C. R.; Caron, K. T.; Chambers, D.; Corstvet, J.; Cowan, E.; de Jesús, V. R.; Espinosa, P.; Fernandez, C.; Holder, C.; Kuklenyik, Z.; Kusovschi, J. D.; Newman, C.; Reis, G. B.; Rees, J.; Reese, C.; Silva, L.; Seyler, T.; Song, M. A.; Sosnoff, C.; Spitzer, C. R.; Tevis, D.; Wang, L.; Watson, C.; Wewers, M. D.; Xia, B.; Heitkemper, D. T.; Ghinai, I.; Layden, J.; Briss, P.; King, B. A.; Delaney, L. J.; Jones, C. M.; Baldwin, G. T.; Patel, A.; Meaney-Delman, D.; Rose, D.; Krishnasamy, V.; Barr, J. R.; Thomas, J.; Pirkle, J. L. Vitamin E Acetate in Bronchoalveolar-Lavage Fluid Associated with EVALI. *N. Engl. J. Med.* **2020**, *382* (8), 697−705.

(3) Dipasquale, M.; Nguyen, M. H. L.; Castillo, S. R.; Dib, I. J.; Kelley, E. G.; Marquardt, D. Vitamin e Does Not Disturb Polyunsaturated Fatty Acid Lipid Domains. *Biochemistry* **2022**, *61* (21), 2366−2376.

(4) Jurak, M.; Miñones Conde, J. Characterization of the Binary Mixed Monolayers of α-Tocopherol with Phospholipids at the Air-Water Interface. *Biochim. Biophys. Acta - Biomembr.* **2013**, *1828* (11), 2410−2418.

(5) Leng, X.; Zhu, F.; Wassall, S. R. Vitamin e Has Reduced Affinity for a Polyunsaturated Phospholipid: An Umbrella Sampling Molecular

Dynamics Simulations Study. *J. Phys. Chem. B* **2018**, *122* (35), 8351−8358.
(6) Muddana, H. S.; Chiang, H. H.; Butler, P. J. Tuning Membrane Phase Separation Using Nonlipid Amphiphiles. *Biophys. J.* **2012**, *102* (3), 489−497.
(7) Keating, E.; Rahman, L.; Francis, J.; Petersen, A.; Possmayer, F.; Veldhuizen, R.; Petersen, N. O. Effect of Cholesterol on the Biophysical and Physiological Properties of a Clinical Pulmonary Surfactant. *Biophys. J.* **2007**, *93* (4), 1391−1401.
(8) Olżyńska, A.; Zubek, M.; Roeselova, M.; Korchowiec, J.; Cwiklik, L. Mixed DPPC/POPC Monolayers: All-Atom Molecular Dynamics Simulations and Langmuir Monolayer Experiments. *Biochim. Biophys. Acta - Biomembr.* **2016**, *1858* (12), 3120−3130.
(9) Wüstneck, R.; Perez-Gil, J.; Wüstneck, N.; Cruz, A.; Fainerman, V. B.; Pison, U. Interfacial Properties of Pulmonary Surfactant Layers. *Adv. Colloid Interface Sci.* **2005**, *117* (1−3), 33−58.
(10) Goerke, J. Pulmonary Surfactant: Functions and Molecular Composition. *Biochim. Biophys. Acta - Mol. Basis Dis.* **1998**, *1408* (2−3), 79−89.
(11) Parra, E.; Pérez-Gil, J. Composition, Structure and Mechanical Properties Define Performance of Pulmonary Surfactant Membranes and Films. *Chem. Phys. Lipids* **2015**, *185*, 153−175.
(12) Casals, C.; Cañadas, O. Role of Lipid Ordered/Disordered Phase Coexistence in Pulmonary Surfactant Function. *Biochimica et Biophysica Acta - Biomembranes.* **2012**, *1818*, 2550−2562. Biochim Biophys Acta November
(13) Lee, K. Y. C.; Majewski, J.; Kuhl, T. L.; Howes, P. B.; Kjaer, K.; Lipp, M. M.; Waring, A. J.; Zasadzinski, J. A.; Smith, G. S. Synchrotron X-Ray Study of Lung Surfactant-Specific Protein SP-B in Lipid Monolayers. *Biophys. J.* **2001**, *81* (1), 572−585.
(14) Behyan, S.; Borozenko, O.; Khan, A.; Faral, M.; Badia, A.; Dewolf, C. Nanoparticle-Induced Structural Changes in Lung Surfactant Membranes: An X-Ray Scattering Study. *Environ. Sci. Nano* **2018**, *5* (5), 1218−1230.
(15) Takamoto, D. Y.; Lipp, M. M.; Von Nahmen, A.; Lee, K. Y. C.; Waring, A. J.; Zasadzinski, J. A. Interaction of Lung Surfactant Proteins with Anionic Phospholipids. *Biophys. J.* **2001**, *81* (1), 153−169.
(16) DiPasquale, M.; Nguyen, M. H. L.; Pabst, G.; Marquardt, D. Partial Volumes of Phosphatidylcholines and Vitamin E: α-Tocopherol Prefers Disordered Membranes. *J. Phys. Chem. B* **2022**, *126* (35), 6691−6699.
(17) Yasmann, A.; Sukharev, S. Properties of Diphytanoyl Phospholipids at the Air−Water Interface. *Langmuir* **2015**, *31* (1), 350−357.
(18) Ładniak, A.; Jurak, M.; Wiącek, A. E. Langmuir Monolayer Study of Phospholipid DPPC on the Titanium Dioxide−Chitosan−Hyaluronic Acid Subphases. *Adsorption* **2019**, *25* (3), 469−476.
(19) Cutro, A. C.; Disalvo, E. A.; Frías, M. A. Effects of Phenylalanine on the Liquid-Expanded and Liquid-Condensed States of Phosphatidylcholine Monolayers. *Lipid Insights* **2019**, *12*, 1−9.
(20) Cheng, S.; Li, S.; Tsona, N. T.; George, C.; Du, L. Insights into the Headgroup and Chain Length Dependence of Surface Characteristics of Organic-Coated Sea Spray Aerosols. *ACS Earth Sp. Chem.* **2019**, *3* (4), 571−580.
(21) Neunert, G.; Hertmanowski, R.; Witkowski, S.; Polewski, K. Effect of Ester Moiety on Structural Properties of Binary Mixed Monolayers of Alpha-Tocopherol Derivatives with DPPC. *Molecules* **2022**, *27* (15), 4670.
(22) Van Bavel, N.; Lai, P.; Loebenberg, R.; Prenner, E. J. Vaping Additives Negatively Impact the Stability and Lateral Film Organization of Lung Surfactant Model Systems. *Nanomedicine* **2022**, *17* (12), 827−843.
(23) Hasegawa, T.; Takeda, S.; Kawaguchi, A.; Umemura, J. Quantitative Analysis of Uniaxial Molecular Orientation in Langmuir-Blodgett Films by Infrared Reflection Spectroscopy. *Langmuir* **1995**, *11* (4), 1236−1243.
(24) Gravel-Tatta, L.; DeWolf, C.; Badia, A. Are Plant-Based Carbohydrate Nanoparticles Safe for Inhalation? Investigating Their Interactions with the Pulmonary Surfactant Using Langmuir Monolayers. *Langmuir* **2021**, *37* (42), 12365−12376.
(25) Borozenko, O.; Faral, M.; Behyan, S.; Khan, A.; Coulombe, J.; Dewolf, C.; Badia, A. Silica Nanoparticle-Induced Structural Reorganizations in Pulmonary Surfactant Films: What Monolayer Compression Isotherms Do Not Say. *ACS Appl. Nano Mater.* **2018**, *1* (9), 5268−5278.
(26) Malcharek, S.; Hinz, A.; Hilterhaus, L.; Galla, H. J. Multilayer Structures in Lipid Monolayer Films Containing Surfactant Protein C: Effects of Cholesterol and POPE. *Biophys. J.* **2005**, *88* (4), 2638−2649.
(27) Brezesinski, G.; Dietrich, A.; Struth, B.; Böhm, C.; Bouwman, W. G.; Kjaer, K.; Möhwald, H. Influence of Ether Linkages on the Structure of Double-Chain Phospholipid Monolayers. *Chem. Phys. Lipids* **1995**, *76* (2), 145−157.
(28) Bringezu, F.; Ding, J.; Brezesinski, G.; Zasadzinski, A. J. Changes in Model Lung Surfactant Monolayers Induced by Palmitic Acid. *Langmuir* **2001**, *17* (15), 4641−4648.
(29) Choi, S. Q.; Kim, K.; Fellows, C. M.; Cao, K. D.; Lin, B.; Lee, K. Y. C.; Squires, T. M.; Zasadzinski, J. A. Influence of Molecular Coherence on Surface Viscosity. *Langmuir* **2014**, *30* (29), 8829−8838.
(30) Gomez-Fernandez, J. C.; Villalain, J.; Aranda, F. J.; Ortiz, A.; Micol, V.; Coutinho, A.; Berberan-Santos, M. N.; Prieto, M. J. E. Localization of A-Tocopherol in Membranes. *Ann. N.Y. Acad. Sci.* **1989**, *570* (1), 109−120.
(31) Layden, J. E.; Ghinai, I.; Pray, I.; Kimball, A.; Layer, M.; Tenforde, M. W.; Navon, L.; Hoots, B.; Salvatore, P. P.; Elderbrook, M.; Haupt, T.; Kanne, J.; Patel, M. T.; Saathoff-Huber, L.; King, B. A.; Schier, J. G.; Mikosz, C. A.; Meiman, J. Pulmonary Illness Related to E-Cigarette Use in Illinois and Wisconsin — Final Report. *N. Engl. J. Med.* **2020**, *382* (10), 903−916.
(32) Baker, M. M.; Procter, T. D.; Belzak, L.; Ogunnaike-Cooke, S. Vaping-Associated Lung Illness (VALI) in Canada: A Descriptive Analysis of VALI Cases Reported from September 2019 to December 2020. *Heal. Promot. Chronic Dis. Prev. Canada* **2022**, *42* (1), 37−44.
(33) Butt, Y. M.; Smith, M. L.; Tazelaar, H. D.; Vaszar, L. T.; Swanson, K. L.; Cecchini, M. J.; Boland, J. M.; Bois, M. C.; Boyum, J. H.; Froemming, A. T.; Khoor, A.; Mira-Avendano, I.; Patel, A.; Larsen, B. T. Pathology of Vaping-Associated Lung Injury. *N. Engl. J. Med.* **2019**, *381* (18), 1780−1781.
(34) Ghosh, A.; Ahmad, S.; Coakley, R. D.; Sassano, M. F.; Alexis, N. E.; Tarran, R. Lipid-Laden Macrophages Are Not Unique to Patients with E-Cigarette or Vaping Product Use-Associated Lung Injury. *Am. J. Respir. Crit. Care Med.* **2021**, *203* (8), 1030−1033.
(35) Milad, N.; Morissette, M. C. Revisiting the Role of Pulmonary Surfactant in Chronic Inflammatory Lung Diseases and Environmental Exposure. *Eur. Respir. Rev.* **2021**, *30* (162), No. 210077.
(36) Ranpara, A.; Stefaniak, A. B.; Williams, K.; Fernandez, E.; LeBouf, R. F. Modeled Respiratory Tract Deposition of Aerosolized Oil Diluents Used in Δ9-THC-Based Electronic Cigarette Liquid Products. *Front. Public Heal.* **2021**, *9* (November), 1−11.

https://doi.org/10.1021/acs.langmuir.3c02952
Langmuir 2024, 40, 5651−5662